Available online at www.sciencedirect.com

SciVerse ScienceDirect

journal homepage: www.elsevier.com/locate/he

Synthesis and hydrogen storage properties of lithium borohydride amidoborane complex

Juner Chen, Teng He, Guotao Wu, Zhitao Xiong, Ping Chen*

Complex Hydride Materials Research Group, Department of Hydrogen Energy and Advanced Materials, Dalian National Laboratory for Clean Energy, Dalian Institute of Chemical Physics, Chinese Academy of Sciences, Dalian 116023, China

ARTICLE INFO

Article history:
Received 25 October 2012
Received in revised form
3 January 2013
Accepted 13 January 2013
Available online 9 February 2013

Keywords:
Hydrogen storage
Lithium borohydride
Lithium amidoborane
Complex
Dehydrogenation

ABSTRACT

A series of mixtures of LiAB/$LiBH_4$ with different molar ratios were prepared and their hydrogen storage properties were investigated in this study. Among them, a new structure was found in the LiAB/$LiBH_4$ sample with a molar ratio of 1/1. It is of orthorhombic structure and composed of alternative layers of LiAB and $LiBH_4$. It shows similar hydrogen desorption behaviors of LiAB–$LiBH_4$ and LiAB–0.5$LiBH_4$. For use in hydrogen storage, high hydrogen capacity and low operation temperature are demanded, thus, the dehydrogenation properties of LiAB–0.5$LiBH_4$ were subsequently measured. Three steps of desorption were observed during the heating process, with a total release of 11.5 wt% H_2 at 500 °C. The reaction path was identified using a combined investigation of XRD and ^{11}B solid state NMR. Dehydrogenation kinetic analyses show that the complex has lower activation energy (61 ± 4 kJ mol^{-1} H_2) than that of LiAB (71 ± 5 kJ mol^{-1} H_2). It is likely that dehydrogenation process was promoted due to the presence of $LiBH_4$.

1. Introduction

Storing hydrogen in solid materials is a promising but challenging way for onboard application in hydrogen fuel cell vehicles. Extensive efforts have been focused on light weight hydrides due to the demand of high hydrogen capacity. Ammonia borane (NH_3BH_3, AB for short), having a hydrogen content of 19.6 wt% is one of most investigated materials [1]. The recently developed metal amidoboranes (MABs), on the other hand, exhibit advantageous dehydrogenation properties over AB. For example, $LiNH_2BH_3$ (LiAB) and $NaNH_2BH_3$ (NaAB) release large amount of hydrogen (10.9 wt% for $LiNH_2BH_3$ and 7.5 wt% for $NaNH_2BH_3$) without borazine formation at 91 °C [2]. The replacement of one H by alkali or alkali earth in AB leads to the transfer of molecular crystal (AB) stabilized by dihydrogen bond to ionic crystal (MAB). Ammonia borane works as a ligand which can bind to lithium cation to form lithium amidoborane-ammonia borane complex with the chemical composition of $LiNH_2BH_3{\cdot}NH_3BH_3$ (LiAB·AB for short), which is composed of alternative layers of LiAB and AB and contains both dihydrogen bond and ionic bond [3]. These findings are useful as guidance for the design and synthesis of other as of yet undiscovered complex hydrides for hydrogen storage.

Lithium borohydride ($LiBH_4$), with a gravimetric density of 18.3 wt% H_2, is a salt-like ionic crystal compound. It decomposes at the temperatures above 300 °C due to its high thermodynamic stability (70 kJ mol^{-1} H_2 [4]) and sluggish kinetic. Intensive activities have been plunged into the modification of $LiBH_4$ to improve its dehydrogenation properties by introducing additives such as oxides [5], carbon [6], metal halides [7,8], metal hydrides [4,9,10], amides [11–14] and etc. Among these, (1−*x*)$LiBH_4$–x$LiNH_2$ system is an interesting one. A series of Li–B–N–H quaternary complex hydrides, such as Li_2BNH_6, $Li_3BN_2H_8$ and $Li_4BN_3H_{10}$, have been prepared and all

* *Corresponding author*. Tel./fax: +86 411 84379583.
E-mail address: wgt@dicp.ac.cn (G. Wu).

0360-3199/$ – see front matter
http://dx.doi.org/10.1016/j.ijhydene.2013.01.094

of them exhibit better dehydrogenation than the parent materials [13–15]. Li_2BNH_6 and $Li_4BN_3H_{10}$ are ionic crystals with a general chemical formula $Li[BH_4]_x[NH_2]_{1-x}$, which can be viewed as three-dimensional frameworks consisting of corner- and face-shared $[Li(BH_4)^-{}_n[(NH_2])^-{}_{4-n}]$ tetrahedral [15]. More recently, new borohydride ammonia borane complexes, such as $Li_2(BH_4)_2NH_3BH_3$, $Ca(BH_4)_2(NH_3BH_3)_2$ were investigated [16]. Both structures are composed of alternating layers of borohydride and ammonia borane stabilized via both dihydrogen bond and ionic bond. However, LiAB–$LiBH_4$ systems are not reported until now. To understand the composition-dependent structure variations and to reveal the hydrogen desorption properties a series of mixtures of LiAB/$LiBH_4$ with different molar ratios were prepared and their hydrogen storage properties were investigated in this study. Among them, a new phase was found in the LiAB/$LiBH_4$ sample with a molar ratio of 1:1. It is worth noting that LiAB–0.5$LiBH_4$ complex showed significant improvement in the dehydrogenation properties, which can release 2 equivalent H_2 faster than LiAB.

2. Experimental

2.1. Sample preparation

$LiNH_2BH_3$ (LiAB) was prepared by ball milling equivalent amount of LiH (98%, Sigma–Aldrich) and NH_3BH_3 (97%, Sigma–Aldrich) in a Retsch PM 400 planetary mill (reaction (1)) [17]. $LiBH_4$ was purchased from Alfa Aesar (95%). In order to determine the composition of new compound, a series of mixtures of LiAB and $LiBH_4$ were prepared by ball milling the starting compounds in different molar ratios of 1/x, with $x = 0.1, 0.2, 0.25, 0.33, 0.5, 1, 2,$ and 10. Approximately 600 mg of sample mixture was loaded into a 180 ml vessel (about 1 bar and 99.9999% Ar inside), which was followed by ball milling at 200 rpm for 2 h. The ball-to-powder ratio was approximately 50:1. For comparison, fresh made LiAB and commercial $LiBH_4$ were both ball milled for 2 h under the same condition. All sample operations were performed in an MBRAUN 200 glovebox filled with argon atmosphere to prevent air contaminations, where O_2 and H_2O concentration were below 10 ppm.

$$LiH + NH_3BH_3 \rightarrow LiNH_2BH_3 + H_2 \quad (1)$$

2.2. Dehydrogenation and characterization

Hydrogen desorption measurements were performed on a homemade temperature programmed desorption (TPD) system combined with mass spectrometer (MS, Hiden HPR-20). Purified argon was employed as a carrier gas in TPD-MS measurements, in which temperature was raised at a ramping rate of 2 °C min^{-1} from 20 to 500 °C. Volumetric release measurements were performed on a Sievert-type apparatus. The reactor was heated from room temperature to 500 °C at a heating rate of 2 °C min^{-1} or held at 80 or 150 °C for isothermal hydrogen release.

X-ray diffraction measurements were conducted upon PANalytical X'pert diffractometer (Cu Kα radiation, 40 kV, 40 mA) to indentify the crystalline phases of the ball-milled samples before and after dehydrogenation. High resolution X-ray diffraction pattern was collected at room temperature at the BL14B1 beamline of Shanghai Synchrotron Radiation Facility (SSRF), Shanghai, China. The obtained data were indexed using TREOR or DICVOL programs. Candidate structures were obtained by performing combined direct space simulated annealing and first principle calculations. Rietveld structural refinement analyses were performed using general structure analysis system (GSAS) [18]. FTIR measurements were conducted on a Varian 3100 FT-IR spectrometer at a resolution of 2 cm^{-1}. Solid-state ^{11}B magic angle spinning nuclear magnetic resonance (MAS NMR) and cross polarization magic angle spinning (CPMAS) experiments were carried out at room temperature on a Bruker AVANCE 500 MHz NMR spectrometer (11.7 T). NMR spectra were generated by Fourier transformation of the free induction decay (FID) following a single pulse excitation without decoupling and a basic cross polarization experiment with arbitrary contact and decoupling schemes, respectively. All of those solid samples were spun at 13 kHz with 4 mm ZrO_2 rotors in diameter, in which the powders were fully loaded. The NMR shifts were reported in parts per million (ppm), externally referenced to $LiBH_4$ at −41.0 ppm for ^{11}B nuclei.

3. Results and discussion

3.1. Sample preparation

Fig. 1 shows the XRD patterns of samples obtained after ball milling LiAB–x$LiBH_4$ with $x = 0.1, 0.2, 0.25, 0.33, 0.5, 1, 2,$ and 10. For comparison, the XRD patterns of the starting materials

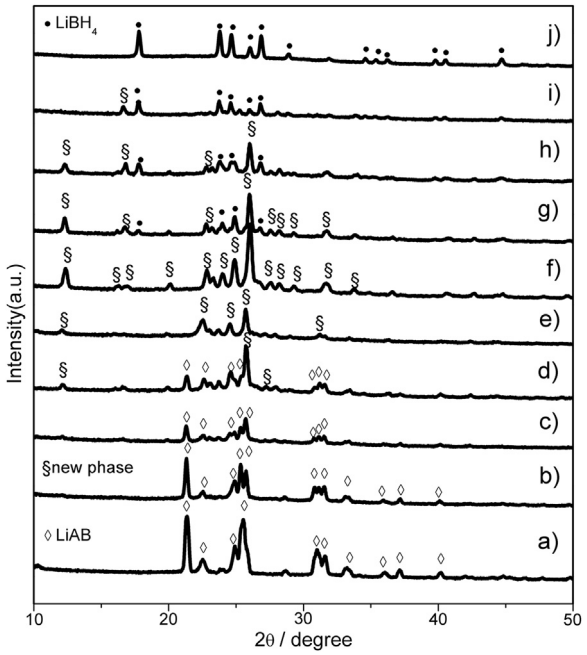

Fig. 1 – XRD patterns of the LiAB–x$LiBH_4$ mixtures with (b) $x = 0.1$, (c) $x = 0.2$, (d) $x = 0.25$, (e) $x = 0.33$, (f) $x = 0.5$, (g) $x = 1$, (h) $x = 2$, (i) $x = 10$, respectively. XRD patterns of (a) as prepared LiAB and (j) commercial $LiBH_4$ are shown for comparison.

are also shown in Fig. 1. A set of diffraction peaks located at $2\theta = 26.0°$, 24.9°, 22.8°, 12.3°, 24.0° etc. were detected in the samples, which cannot match with any known compound. It is likely that a new compound was formed during the ball milling process. As shown in Fig. 1, diffraction peaks of LiAB are detectable for samples with $x < 0.33$; meanwhile, diffraction peaks of $LiBH_4$ are detectable if x is larger than 2. So the composition of new compound is likely in the range of $x = 0.5–1$. The structures of LiAB–x$LiBH_4$ were further verified by the FTIR characterizations. As shown in Figure S1, absorbances from 3400 cm^{-1} to 3200 cm^{-1} and from 2400 cm^{-1} to 2100 cm^{-1} are associated with the stretching of N–H and B–H bonds, respectively. Absorbances at around 1570 cm^{-1} and 1200 cm^{-1} are associated with the bending of N–H and B–H bonds, respectively. Compared with LiAB and $LiBH_4$, the FTTR spectra of LiAB–$LiBH_4$ obviously exhibits different vibrational features while LiAB–0.5$LiBH_4$ still have characteristic N–H stretch of LiAB of $NH_2BH_3^-$, and thus, LiAB–$LiBH_4$ (1/1) should be the right composition of the new phase.

The diffraction peaks of the new compound can be indexed using an orthorhombic cell with space group *Pbca* and lattice parameters of $a = 9.2824(18)$ Å, $b = 14.3092(28)$ Å, $c = 7.6194(12)$ Å and $V = 1012.0(3)$ $Å^3$. BH_4^- and $NH_2BH_3^-$ were treated as rigid bodies. First-principles calculations were used to identify the positions of hydrogen atoms in the structure. In $Li_2(BH_4)(NH_2BH_3)$ crystal, LiAB layer and $LiBH_4$ layer are arranged perpendicular to the *b*-axis alternatively, which is similar to the structure of β-LiAB [2]. The strong intermolecular interaction is derived from the ionic bondings among Li^+ cations, $NH_2BH_3^-$ anions and BH_4^- anions. Li cations are located in two tetrahedral coordination positions. One is bonded with one NH_2 group of $NH_2BH_3^-$, two BH_3 groups of $NH_2BH_3^-$ and one BH_4^-, the other is bonded with three BH_4^- and one BH_3 of $NH_2BH_3^-$ as shown in Fig. 2. In addition, the calculated distances of NH···HB is in the range of 2.181–2.387 Å, which suggests that dihydrogen bonds also exist in the crystal. The detailed structural information is shown in the supplementary information.

3.2. *Dehydrogenation of LiAB–0.5$LiBH_4$*

Dehydrogenation properties of the complexes LiAB–x$LiBH_4$ ($x = 0.5$ and 1) were investigated by temperature programmed desorption (TPD). As shown in Figure S3, it is illustrated that three steps of hydrogen release were observed during the heating process, and it shows similar hydrogen desorption behaviors of both two complexes below 150 °C. For use in hydrogen storage, high hydrogen capacity and low operation temperature are demanded, thus, materials with more hydrogen release at lower temperature are favorable. In this study, samples with more LiAB may have more hydrogen to release. Hence, the dehydrogenation properties of the complex LiAB–0.5$LiBH_4$ were subsequently measured. Fig. 3 shows volumetric release and TPD-MS results of the sample. The MS-H_2 data of starting materials, LiAB and $LiBH_4$, are also shown in Fig. 3b1 for comparison. The total desorption capacity of LiAB–0.5$LiBH_4$ up to 500 °C is 2.75 equivalences or 11.5 wt% of hydrogen (Fig. 3a). The onset dehydrogenation temperature of LiAB–0.5$LiBH_4$ was decreased to 65 °C, lower than that of LiAB, suggesting that the presence of $LiBH_4$ may be a promoter factor to improve the dehydrogenation properties of LiAB–0.5$LiBH_4$ complex. The promotion may be caused by the formation of a new layer structure complex and the particle size decrease due to a higher efficiency of ball milling the mixture of LiAB and $LiBH_4$ than that of ball milling LiAB alone. Three peaks of hydrogen evolution can be observed at ca. 75, 100, and 395 °C without any detectable borazine, ammonia and diborane signals in the MS tracks within the temperature range of 20–500 °C. Corresponding to the dehydrogenation amount as shown in Fig. 3a, the first step shows a higher dehydrogenation rate, which gives off one equivalent hydrogen below 80 °C. When heated up to 150 °C, additional equivalent hydrogen was released in the second step. The third step dehydrogenation may be related to the decomposition of $LiBH_4$. However, the peak temperature is notably lower than that of $LiBH_4$.

To clarify the reactions occur in dehydrogenation process, we carried out XRD and NMR characterizations on the post-dehydrogenated samples after releasing 1.0, 2.0, and 2.75 equivalents H_2, respectively. Unfortunately, all dehydrogenated samples are amorphous except that crystalline LiH was detected by XRD in the dehydrogenation samples collected at 500 °C as shown in Figure S4.

^{11}B solid state NMR spectra give more information about those amorphous dehydrogenated samples. As shown in Fig. 4, two resonances observed in the ^{11}B MAS and CPMAS NMR spectra at −21.6 and −40.5 ppm of the fresh made LiAB–0.5$LiBH_4$ can be ascribed to sp^3 hybridized B elements, [NBH_3] and [BH_4], respectively [19,20]. After releasing 1.0 equivalent hydrogen it was found that ^{11}B resonances belong to [NBH_3] and [BH_4] were still detectable. Two new resonances at 27.0 and 20.9 ppm were observed in MAS NMR spectra, which belong to sp^2 hybridized B elements, [BN_3] and/or [N_2BH] [21]. There is no clear ^{11}B signal in the range of 0 to −20 ppm. Further desorption of the second equivalent hydrogen results in the depletion of [NBH_3] species. However, the ^{11}B MNR signal of [BH_4] still remains and downshifts 0.8 ppm. After releasing 2.75 equivalent H_2, the sample presents only two broad peaks centered at 24.5 and 16.6 ppm. The disappearance of [BH_4] suggests the decomposition of $LiBH_4$. It is worth noting that there is no ^{11}B CPMAS NMR signal in the range of 15 ppm–30 ppm, which indicates that the product may be BN after the dehydrogenation at 500 °C.

A possible mechanism of dehydrogenation may be described by the following reactions:

$$LiNH_2BH_3 - 0.5LiBH_4 \rightarrow [LiNBH] + 0.5LiBH_4 + 2H_2 \quad (2)$$

$$[LiNBH] + 0.5LiBH_4 \rightarrow 1.5LiH + [BN] + 0.5B + 0.75H_2 \quad (3)$$

3.3. *Kinetic analysis*

To shine a light on the thermodynamic and kinetic properties of dehydrogenation of the combined and pristine samples, LiAB–0.5$LiBH_4$ and LiAB underwent volumetric release at 80 and 150 °C, respectively. The dehydrogenation of the first equivalent hydrogen from LiAB was fast but the second step was quite slow at 80 °C. For LiAB–0.5$LiBH_4$, as shown in Figure S5, ca. 2.0 equivalents H_2 can be released in about 480 min and 24 min at 80 and 150 °C, respectively. It illustrates

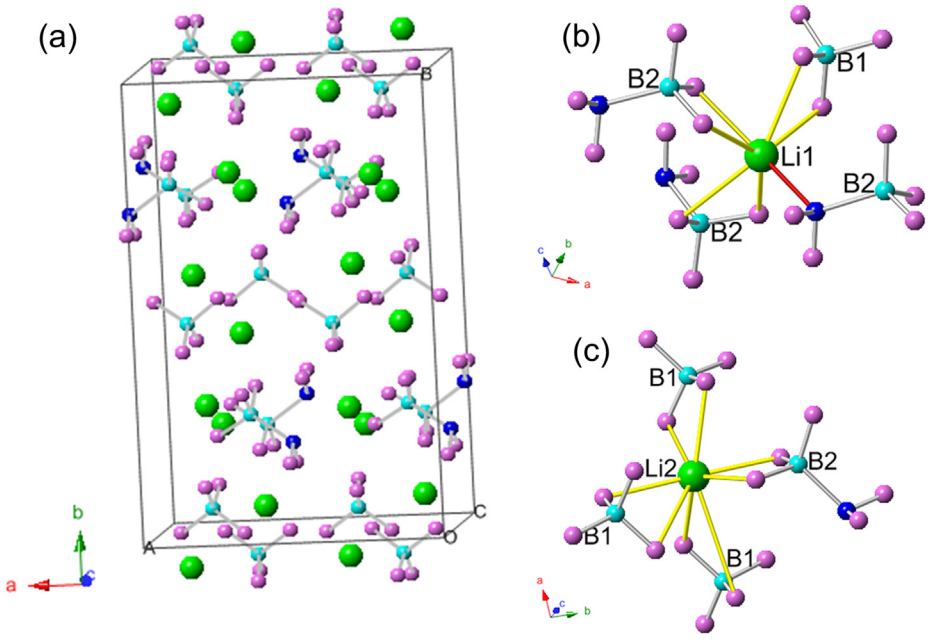

Fig. 2 – (a) Crystal structure of $Li_2[BH_4][NH_2BH_3]$ and (b, c) close contacts around the Li^+ center in $Li_2[BH_4][NH_2BH_3]$ structure. Lithium is represented by green spheres, nitrogen by blue spheres, boron by cyan spheres, and hydrogen by pink spheres. (For interpretation of the references to color in this figure legend, the reader is referred to the web version of this article.)

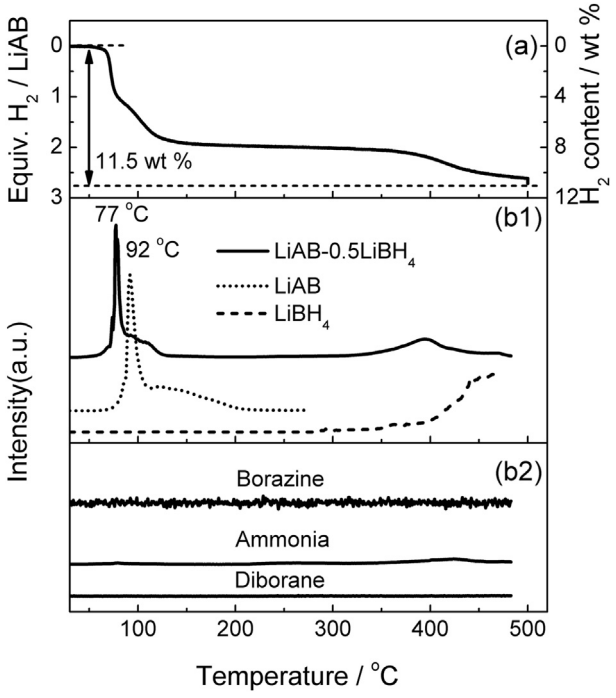

Fig. 3 – (a) Volumetric release measurement on LiAB–0.5$LiBH_4$. (b) TPD-MS results: (b1), H_2 signal of LiAB–0.5$LiBH_4$ sample. For comparison, H_2 signals of LiAB (dot line) and $LiBH_4$ (dash line) are also shown; (b2) Borazine, ammonia, and diborane signals of LiAB–0.5$LiBH_4$.

that LiAB–0.5$LiBH_4$ has a higher dehydrogenation rate than that of LiAB. Therefore, the energy barrier should be reduced due to the formation of the complex LiAB–0.5$LiBH_4$. JMA equation was used to describe the time-dependent kinetic behaviors for isothermal dehydrogenation of LiAB–0.5$LiBH_4$ and LiAB at 80 °C, see in supporting information, which indicated that the rate limiting processes in the initial stage of

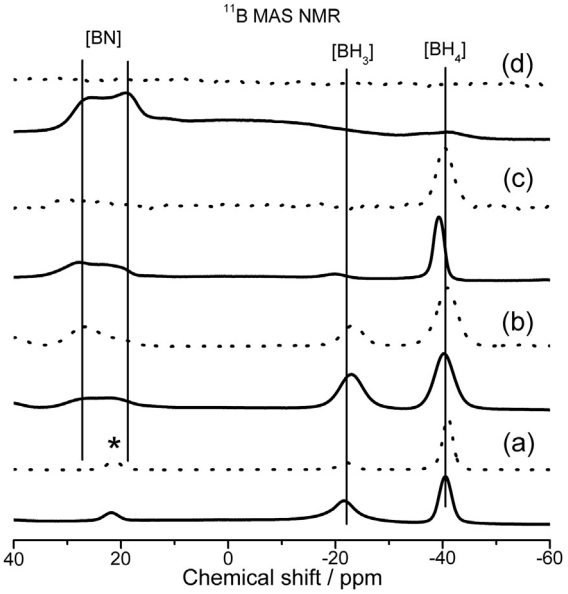

Fig. 4 – ^{11}B MAS (solid lines) and CPMAS (dot lines) NMR spectra of (a) fresh-made LiAB–0.5$LiBH_4$ and samples after releasing (b) 1.0 equivalent H_2; (c) 2.0 equivalent H_2; (d) 2.75 equivalent H_2 per LiAB, respectively. Asterisk denotes spinning side bands.

dehydrogenation of LiAB–0.5LiBH$_4$ and LiAB were corresponding to three-dimensional growth of nuclei and a diffusion controlled reaction, respectively. So the diffusion process during dehydrogenation of LiAB–0.5LiBH$_4$ may become easier than that of LiAB.

To obtain the distinctly enhanced kinetics of LiAB–0.5LiBH$_4$, we adopted Kissinger's method (equation (4)) to determine the kinetic barrier in hydrogen desorption.

$$\ln\left(\beta/T_p^2\right) = -E_a/RT_p + \ln(AR/E_a) \quad (4)$$

Here T_p is the temperature at which the maximum reaction rate peaks, β is the heating rate, E_a is the activation energy, A is the pre-exponential factor, and R is the gas constant. The maximum reaction-rate temperatures at different heating rates were collected by means of TPD measurements. The TPD profiles of hydrogen desorption from the LiAB–0.5LiBH$_4$ and LiAB samples at different ramping rates are shown in Fig. 5. It was observed that the peak temperatures shifted monotonically to higher values when the ramping rate was increased from 2 to 8 K min^{-1}. The dependence of $\ln(\beta/T_p^2)$ to $1/T_p$ was plotted (shown in Fig. 5). The slope and the intercept of the fitted line are used to determine the values of E_a and A, respectively. Once E_a and A are known, the specific rate constant k at given temperature can be determined by the Arrhenius equation

$$k = A\exp(-E_a/RT) \quad (5)$$

E_a, A, and k (at 80 °C) for LiAB–0.5LiBH$_4$ and LiAB are shown in Table 1. As mentioned above, the rate constant k at 80 °C of LiAB–0.5LiBH$_4$ is larger than that of LiAB, which agrees with the observation on the higher rate of hydrogen release in isothermal volumetric release measurements. The activation energy E_a for hydrogen desorption from the LiAB–0.5LiBH$_4$ is around 61 ± 4 kJ mol^{-1} which is ca. 14% lower than that of LiAB (71 ± 5 kJ mol^{-1}), suggesting a considerable enhancement in dehydrogenation kinetics of LiAB after complexed with LiBH$_4$.

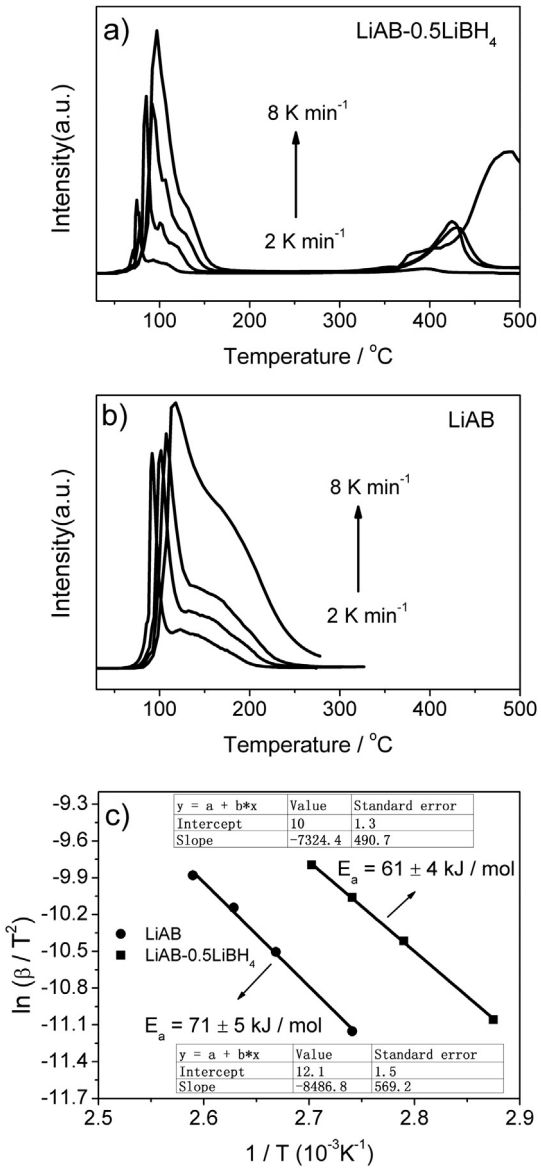

Fig. 5 – TPD profiles of hydrogen desorption from (a) LiAB–0.5LiBH$_4$ and (b) LiAB at ramping rates of 2, 4, 6, and 8 K min^{-1}, respectively. (c) The Kissinger's plots, which give the activation energy of hydrogen release from the LiAB–0.5LiBH$_4$ and LiAB samples.

Table 1 – E_a, A, and k (at 80 °C) calculated from the Kissinger equation and Arrhenius equation.

	E_a (kJ mol^{-1})	A (min^{-1})	k (min^{-1})
LiAB–0.5LiBH$_4$	61 ± 4	1.7 × 10^8	1.6 × 10^{-1}
Pristine LiAB	71 ± 5	1.7 × 10^9	5.7 × 10^{-2}

4. Conclusions

In the present study, a new complex of LiAB–LiBH$_4$ was synthesized, which has an orthorhombic structure and is composed of alternative layers of LiAB and LiBH$_4$. The dehydrogenation properties of LiAB–0.5LiBH$_4$ were systematically investigated. It was found that hydrogen was released through three steps and with a low onset dehydrogenation temperature of ca. 65 °C. The reactions occurred during the dehydrogenation process were studied using a combination of XRD and ^{11}B solid state NMR. In the first two steps, hydrogen mainly comes from LiAB component, while the last step is related to the decomposition of LiBH$_4$. The dehydrogenation kinetics was investigated by Kissinger's method. It was found that the complex LiAB–0.5LiBH$_4$ has lower activation energy (E_a = 61 ± 4 kJ mol^{-1}) and higher rate (k = 1.6 × 10^{-1} min^{-1}) than LiAB (E_a and k) in hydrogen desorption.

Acknowledgments

We acknowledge the financial support from National Natural Science foundation of China (50901070, 10979051, 20971120, 20973162 and U1232120), Hundred Talents Project and Knowledge Innovation Program of CAS (KJCX3-YW-H21) and the National Basic Research Program of China (2010CB631304).

The authors wish to thank BL14B1 of Shanghai Synchrotron Radiation Facility (SSRF) for providing the beam time.

Appendix A. Supplementary data

Supplementary data related to this article can be found at http://dx.doi.org/10.1016/j.ijhydene.2013.01.094.

REFERENCES

[1] Denney MC, Pons V, Hebden TJ, Heinekey DM, Goldberg KI. Efficient catalysis of ammonia borane dehydrogenation. Journal of the American Chemical Society 2006;128:12048–9.

[2] Xiong Z, Yong CK, Wu G, Chen P, Shaw W, Karkamkar A, et al. High-capacity hydrogen storage in lithium and sodium amidoboranes. Nature Materials 2007;7:138–41.

[3] Wu C, Wu G, Xiong Z, Han X, Chu H, He T, et al. $LiNH_2BH_3{\cdot}NH_3BH_3$: structure and hydrogen storage properties. Chemistry of Materials 2009;22:3–5.

[4] Vajo JJ, Skeith SL, Mertens F. Reversible storage of hydrogen in destabilized $LiBH_4$. The Journal of Physcial Chemistry B 2005;109:3719–22.

[5] Zuttel A, Rentsch S, Fischer P, Wenger P, Sudan P, Mauron P, et al. Hydrogen storage properties of $LiBH_4$. Journal of Alloys and Compounds 2003;356:515–20.

[6] Fang ZZ, Kang XD, Dai HB, Zhang MJ, Wang P, Cheng HM. Reversible dehydrogenation of $LiBH_4$ catalyzed by as-prepared single-walled carbon nanotubes. Scripta Materialia 2008;58:922–5.

[7] Arnbjerg LM, Ravnsbæk DB, Filinchuk Y, Vang RT, Cerenius Y, Besenbacher F, et al. Structure and dynamics for $LiBH_4$–LiCl solid solutions. Chemistry of Materials 2009;21:5772–82.

[8] Martelli P, Remhof A, Borgschulte A, Ackermann R, Strassle T, Embs JP, et al. Rotational motion in $LiBH_4$/LiI solid solutions. The Journal of Physical Chemistry A 2011;115:5329–34.

[9] Mauron P, Bielmann M, Remhof A, Zuttel A, Shim J-H, Cho YW. Stability of the $LiBH_4/CeH_2$ composite system determined by dynamic PCT measurements. The Journal of Physical Chemistry C 2010;114:16801–5.

[10] Yang J, Sudik A, Wolverton C. Destabilizing $LiBH_4$ with a metal (M = Mg, Al, Ti, V, Cr, or Sc) or metal hydride (MH_2, MgH_2, TiH_2, or CaH_2). The Journal of Physical Chemistry C 2007;111:19134–40.

[11] Aoki M, Miwa K, Noritake T, Kitahara G, Nakamori Y, Orimo S, et al. Destabilization of $LiBH_4$ by mixing with $LiNH_2$. Applied Physics A-Materials Science & Processing 2005;80:1409–12.

[12] Noritake T, Aoki M, Towata S, Ninomiya A, Nakamori Y, Orimo S. Crystal structure analysis of novel complex hydrides formed by the combination of $LiBH_4$ and $LiNH_2$. Applied Physics A-Materials Science & Processing 2006;83:277–9.

[13] Pinkerton FE, Meisner GP, Meyer MS, Balogh MP, Kundrat MD. Hydrogen desorption exceeding ten weight percent from the new quaternary hydride $Li_3BN_2H_8$. The Journal of Physical Chemistry B 2004;109:6–8.

[14] Zheng X, Xiong Z, Lim Y, Wu G, Chen P, Chen H. Improving effects of LiH and Co-catalyst on the dehydrogenation of $Li_4BN_3H_{10}$. The Journal of Physical Chemistry C 2011;115:8840–4.

[15] Wu H, Zhou W, Udovic TJ, Rush JJ, Yildirim T. Structures and crystal chemistry of Li_2BNH_6 and $Li_4BN_3H_{10}$. Chemistry of Materials 2008;20:1245–7.

[16] Wu H, Zhou W, Pinkerton FE, Meyer MS, Srinivas G, Yildirim T, et al. A new family of metal borohydride ammonia borane complexes: synthesis, structures, and hydrogen storage properties. Journal of Materials Chemistry 2010;20:6550.

[17] Wu GT, Wu CZ, Xiong ZT, David WIF, Ryan KR, Jones MO, et al. Stepwise phase transition in the formation of lithium amidoborane. Inorganic Chemistry 2010;49:4319–23.

[18] Larson AC, Von Dreele RB. GSAS. General structure analysis system. Los Alamos, New Mexico: LANSCE, MS-H805; 1994.

[19] Bluhm ME, Bradley MG, Butterick R, Kusari U, Sneddon LG. Amineborane-based chemical hydrogen Storage: enhanced ammonia borane dehydrogenation in ionic liquids. Journal of the American Chemical Society 2006;128:7748–9.

[20] Kim D-P, Moon K-T, Kho J-G, Economy J, Gervais C, Babonneau F. Synthesis and characterization of poly(aminoborane) as a new boron nitride precursor. Polymers for Advanced Technologies 1999;10:702–12.

[21] Gervais C, Framery E, Duriez C, Maquet J, Vaultier M, Babonneau F. ^{11}B and ^{15}N solid state NMR investigation of a boron nitride preceramic polymer prepared by ammonolysis of borazine. Journal of the European Ceramic Society 2005;25:129–35.